Archives of Acoustics Vol. 49, No. 1, pp. 73–81 (2024), doi: 10.24425/aoa.2024.148769

Research Paper

Design and Verification of Sector Vortex Archimedean Spiral Phased Array Transducer for Improving Focus Acoustic Pressure

Xiaodan LU[(1)], Deping ZENG[(1),(2)*]

[(1)] *State Key Laboratory of Ultrasound in Medicine and Engineering, College of Biomedical Engineering Chongqing Medical University*
Chongqing, China

[(2)] *National Engineering Research Center of Ultrasound Medicine*
Chongqing, China

*Corresponding Author e-mail: 102300@cqmu.edu.cn

(*received April 8, 2023; accepted October 3, 2023; published online January 8, 2024*)

The emergence of high-intensity focused ultrasound applications brings great potential to establish non-invasive therapeutic treatment in place of conventional surgery. However, the development of ultrasonic technology also poses challenges to the design and manufacture of high-power ultrasound transducers with sufficient acoustic pressure. Here, the design of a sector vortex Archimedean spiral phased array transducer that is able to enhance focal acoustic pressure is proposed by maximizing the filling factor of the piezoelectric array. The transducer design was experimentally verified by hydrophone measurements and matched well with acoustic simulation studies. The focal deflection was shown to be feasible up to ±9 mm laterally and up to ±20 mm axially, where the effective focal acoustic pressure can be maintained above 50% and the level of the grating lobe below 30%. Furthermore, a homogeneous pressure distribution without secondary focus was observed in the pre-focal region of the transducer. The rational design of a high-intensity focused ultrasound transducer indicates promising development in the treatment of deep tissue thermal ablation for clinical applications.

Keywords: phased array transducer; Archimedean spiral; high-intensity focused ultrasound (HIFU); focal deflection.

1. Introduction

High-intensity focused ultrasound (HIFU) is rapidly developing as an ideal non-invasive alternative to conventional surgery, by using the good penetrability of ultrasound waves in human tissues. HIFU can be used for the treatment of benign and malignant solid tumors, providing a non-invasive and green treatment technology with broad development prospects. Clinically, this technology has been used to treat uterine fibroids (Liu *et al.*, 2017), liver cancer (Fukuda *et al.*, 2011), breast cancer (Feril *et al.*, 2021), etc. To enable effective HIFU treatment, the ultrasound transducer plays a pivotal role in precisely focusing the ultrasound on the tumor tissue in the human body and forming a high temperature above 65°C in the target area within a short time. The thermal effect, mechanical effect, and cavitation effect of ultrasound at the focus synergistically cause protein denaturation, coagulative necrosis of tissue cells, or irreversible serious damage. This achieves the objective of treating tumors without damaging the surrounding tissues (Shehata Elhelf *et al.*, 2018).

Among the currently available transducers, the phased array transducer is an ideal candidate for delivering focused ultrasonic waves in HIFU treatment. It consists of multiple piezoelectric elements, each with a specific excitation signal. By controlling the phase of the element excitation signals, single or muti-focus as well as axial or lateral focal deflection can be achieved without moving the transducer. Assisted by electronic focusing, the ultrasonic beam can move flexibly and

quickly to track the movement of organs, for example, the kidney and liver during breathing. In addition, wave aberration can be compensated by heterogeneous media to avoid obstacles such as ribs and forming multiple lesions (Auboiroux *et al.*, 2011; Lean, Zhou, 2019).

In clinical applications, the critical requirements for HIFU usage are: 1) providing high focal acoustic pressure; 2) reducing levels of sidelobe and grating lobe; 3) increasing the focal deflection range to ensure sufficient focal intensity for deep tissue thermal ablation. However, problems in phased array focused ultrasonic devices include an acoustic pressure decreases and the occurrence of excessive grating lobe caused by focus deflection. Leading to thermal damage in the proximal region (such as the skin). Particularly, this effect becomes pronounced as the distance of focal deflection increases (Ebbini, Cain, 1991).

To improve focus quality, especially for deep tissue thermal ablation, the rational design of a phased array transducer should follow several principles, including a large aperture and close packing of single elements, where the distance between each element center should not exceed half of the wavelength (Hynynen, Jones, 2016; Ramaekers *et al.*, 2017a). In earlier studies, regular and periodic arrays were used, leading to an excessively high level of the grating lobe limiting focal deflection (Daum, Hynynen, 1999; Goss *et al.*, 1996). Later, Goss *et al.* (1996) introduced random arrays to optimize array performance and effectively reduce the level of the grating lobe. Gavrilov and Hand (2000) compared the acoustic field between regular and random arrays through a numerical simulation and element size modification. The authors confirmed improved focal quality in random arrays, while a lower focal acoustic pressure was observed attributed to the low filling factor of the elements. In 2015, Gavrilov *et al.* proposed the spiral array arrangement as a solution to increase the intensity of focus and suggested that the filling factor of elements directly affected the intensity of the focus acoustic pressure. Therefore, the spiral array is one of the solutions to the above problems. Notably when the piezoelectric material is constrained by power limitations, the radiation area of the transducer should be increased as much as possible (Rosnitskiy *et al.*, 2020), so that the active surface of the transducer and the close filling of elements contribute in achieving the desired focal acoustic pressure and spread the generated acoustic pressure uniformly in the pre-focal region to avoid damage caused by undesired hotspots (Payne *et al.*, 2011).

Furthermore, compared to other spiral structures (16-spirals (Rosnitskiy *et al.*, 2018), Fermat's spiral (Ramaekers *et al.*, 2017b), etc.), the Archimedean spiral phased array provides a simple structure, flexible element arrangement, and a wider deflection range (Morrison *et al.*, 2014). Wang *et al.* (2021) proposed an Archimedean spiral PMUT array, which can generate greater axial acoustic pressure, with acoustic emission pressure 18% higher than that of traditional array structure. However, in current studies, most elements of the Archimedean spiral array are in circular shape, resulting in relatively low filling factors of the array. Therefore, in this work, we sought a novel approach to build a high-power phased array transducer with a small number of transducer elements while allowing sufficient focal deflection and maintaining simplicity in design.

Our research approach is to restrict the number of array elements to 128 and improve the design of the Archimedean spiral array by using sector vortex elements to further increase the filling factor. These elements were distributed on a spherical crown with an opening diameter of 200 mm and a radius of curvature of 180 mm. In the authors' previous research (Lu, Zeng, 2023), the improved focal acoustic pressure was demonstrated through simulations and compared to a configuration with circular elements, the obtained focal acoustic pressure in the sector vortex elements was 32.28% higher compared to the circular configuration. Consequently, according to the simulated structural parameters, a sector vortex Archimedean spiral phased array transducer that met the requirements was fabricated, the acoustic performance of the transducer was validated in acoustic field scanning experiments and the results were compared with acoustic simulations. This research provides feasible promises for the design and optimization of focused ultrasonic transducers.

2. Materials and method

2.1. Array design

Figure 1 shows the design of the 128-sector vortex Archimedean spiral array studied in this work. The sector vortex array elements are closely distributed on a spherical crown with an opening diameter of 200 mm, a radius of curvature of 180 mm, and 7.5 turns of Archimedean spiral. A circular hole with an inner diameter of 60 mm at the center is cut out to allow the B-ultrasound probe for image monitoring. The number of array elements is set to 128. The design of the array

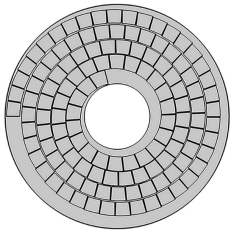

Fig. 1. Illustration of the 128-sector vortex Archimedean spiral phased array transducer design.

elements shape was first generated on a planar surface (Raju *et al.*, 2011) and then projected through the center onto a spherical crown with a radius of curvature 180 mm to ensure that the areas of elements were uniform. On the spherical crown, the projected area of a single sector vortex element was 173.35 mm^2, and a filling factor of the elements was about 70.55%. The filling factor can be calculated using Eq. (1) (Rosnitskiy *et al.*, 2020), where Σ_{act} is the sum of the effective areas of all array elements, and Σ is the total area of spherical crown radiation. Specific parameters of the 128-sector vortex Archimedean spiral phased array transducer are shown in Table 1:

$$\Psi = \left(\frac{\Sigma_{\text{act}}}{\Sigma}\right) \times 100\%. \tag{1}$$

Table 1. Parameters of Archimedean spiral phased array transducer.

Number of elements	Opening diameter [mm]	Inner diameter [mm]	Radius of curvature [mm]
128	200	60	180
F number	Shape of elements	Spiral turns	Filling factor
0.9	sector vortex	7.5	70.55%

2.2. Acoustic simulation

The acoustic fields of the 128-sector vortex Archimedean spiral phased array transducer were simulated by finite element analysis. The simulations only modeled linear acoustic effects, which were sufficient to evaluate the focal deflection capabilities of various array designs. The frequency of the acoustic simulations was taken as 1 MHz. Assuming that the propagation medium is homogeneous, the density of water was considered as 1000 kg/m^3, and the speed of sound as 1500 m/s. A pressure of 1 Pa was applied to each array element, and finally, the size of each grid was adjusted to a minimum of $\lambda/8$ and a maximum of $\lambda/6$, where λ is the wavelength.

2.3. Transducer fabrication

The single element of the array is made of P8-type piezoelectric ceramic, with the concave side being the negative electrode and the convex side being the positive electrode, and the frequency of the transducer is 1 MHz. The shell contains 128 mounting points to hold the element assembly in a suitable place, and the elements are connected by positive and negative electrode leads. The center hole of the shell and the array allow for the placement of a B-ultrasound probe for image monitoring, further enhancing the practicability of the transducer. An image of the as-fabricated 128-sector vortex Archimedean spiral phased array transducer is shown in Fig. 2.

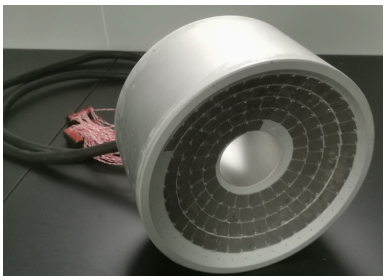

Fig. 2. Image of the as-fabricated 128-sector vortex Archimedean spiral phased array transducer.

2.4. Hydrophone measurements

Hydrophone measurements were performed in a degassed water tank with the as-fabricated transducer and compared with the acoustic simulation to verify the acoustic performances. The whole measurement system contained the phased array control system, the acoustic field scanning system, and the three-dimensional motion system, as shown in Fig. 3. In the experiment, the transducer was immersed in degassed water, the surface of the transducer was perpendicular to the hydrophone, and the upper computer software controlled the 128-channel digital generator to produce signals driving the transducer to transmit ultrasonic waves. The hydrophone was moved by a three-dimensional stepping motor to scan and measure in three orthogonal directions with a step length of 0.1 mm, acquiring and processing the signal. The measured signal voltage was converted into acoustic pressure through the sensitivity provided by the hydrophone manufacturer. To evaluate the focal deflection capability, the delay time was calculated based on known array element coordinates to control the focus deflection in three orthogonal directions. This process allows to determine changes in focus acoustic pressure, levels of the sidelobe and grating lobe, and focal plane acoustic pressure distributions. Furthermore, focal plane acoustic pressure distributions were obtained at 15, 25, and 50 mm in the pre-focal region to observe the pre-focal acoustic pressure distribution.

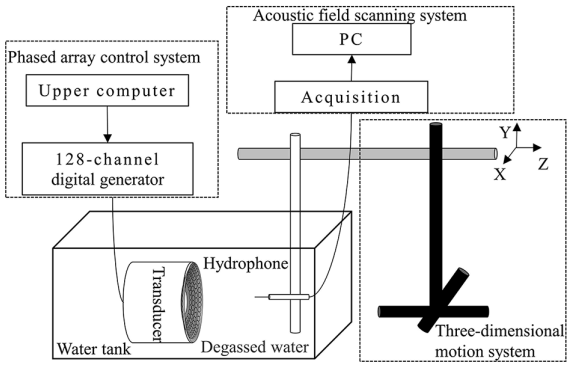

Fig. 3. Schematic diagram of the acoustic field measurement device.

3. Results and discussion

3.1. Focusing at the geometric focus

Figure 4 illustrates the one-dimensional normalized acoustic pressure distributions at the geometric focus obtained in three orthogonal directions, obtained through hydrophone measurements and acoustic simulations under free-field conditions. It can be seen that the results between the hydrophone measurements and acoustic simulations are in good agreement, demonstrating symmetry in positive and negative directions. Specifically, the experimental results exhibit sidelobe levels of 21% laterally (Figs. 4a and 4b) and 24% axially (Fig. 4c), while the simulation values of 25% and 19%, respectively, with a maximum error of 5%. No evidence of strong sidelobes and grating lobe approaching −10 dB of the main lobe is observed. Furthermore, Figs. 4a and 4b show that the sidelobe levels of the experimental results are lower than the simulation results, which is likely because of the inevitable imperfect manufacturing process of the actual transducer implementation, including the loss of regularity in element placement, thereby improving the performance of acoustic field distribution.

3.2. Focal deflection capability

According to the criteria for assessing the focal deflection capability of phased array transducers established in earlier studies (Ebbini, Cain, 1991; Ramaekers *et al.*, 2017a; Rosnitskiy *et al.*, 2018), focal deflection is effective when the decrease in acoustic pressure after focal deflection is less than 50% and it is safe if the level of the grating lobe is less than 30% when the focus is deflected. In this work, the measurements for each point are normalized and evaluated according to this criterion (the dashed lines in Figs. 5 and 6 are the standard thresholds).

Figure 5 illustrates the focal acoustic pressure obtained by the hydrophone measurements and acoustic simulations after controlling the focus deflected in three orthogonal directions under free-field conditions. The focus is deflected up to ±10 mm in steps of 2 mm

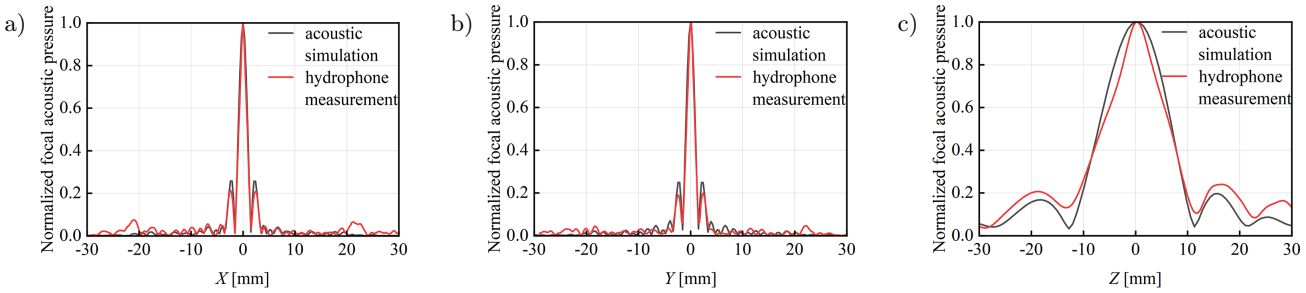

Fig. 4. Illustration of the one-dimensional normalized acoustic pressure distributions at the geometric focus on the X-axis (a), the Y-axis (b), and the Z-axis (c), obtained by the hydrophone measurements and the acoustic simulations.

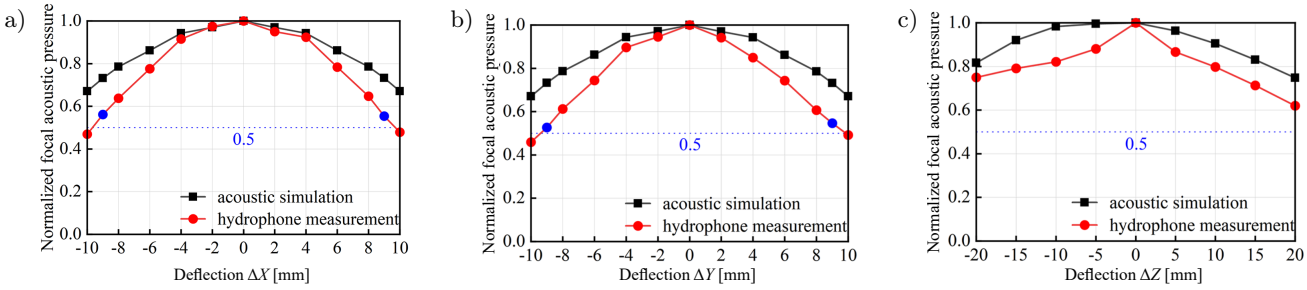

Fig. 5. Illustration of the normalized focus acoustic pressure levels deflected on the X-axis (a), the Y-axis (b), and the Z-axis (c), obtained by the hydrophone measurements and the acoustic simulations.

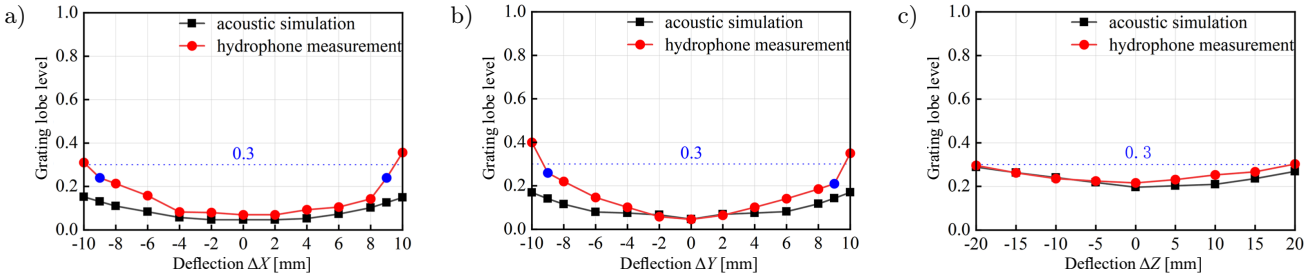

Fig. 6. Illustration of the grating lobe levels for focus deflected on the X-axis (a), the Y-axis (b), and sidelobe levels for focal deflected on the Z-axis (c), obtained by the hydrophone measurements and the acoustic simulations.

on the X-axis (Fig. 5a) and Y-axis (Fig. 5b), and up to ±20 mm in steps of 5 mm on the Z-axis (Fig. 5c). A good symmetry between the positive and negative deflections of the focus is observed, and as the focal deflection distance increases, the focal acoustic pressure decreases linearly. The blue dots in Figs. 5a and 5b indicate that focal deflection appears to be feasible for lateral deflections up to ±9 mm, where the focal acoustic pressure level is reduced by approximately 45%. At ±10 mm, the pressure level drops by more than 50%, however, in the acoustic simulations this drop is 33%. In Fig. 5c, the acoustic pressure reductions of 25% for the negative direction and 38% for the positive direction are observed in experimental results for the focal deflection up to ±20 mm on the Z-axis. These values are 5% and 10% higher than the acoustic simulations. Therefore, the focal pressure reductions and the margin of error are smaller compared to those observed for lateral deflections.

Figure 6 illustrates the levels of the grating lobe and sidelobe corresponding to Fig. 5. When the focus is deflected up to ±10 mm, the proportion of positive and negative grating lobe levels increases from 7 to 35 and 31%, respectively, on the X-axis (Fig. 6a), and increases from 4.6 to 35 and 40%, respectively, on the Y-axis (Fig. 6b), while the results of the acoustic simulations are less than 17%. Therefore, the blue dots in Figs. 6a and 6b show that the proportion of the grating lobe is less than 26% at ±9 mm on the lateral axis, which satisfies the safety standard. When the focus is deflected up to ±20 mm, the sidelobe levels are less than 29% on the Z-axis (Fig. 6c), and the margin of error is less than 3% compared to the acoustic simulations. Thus, the results of hydrophone measurements on the Z-axis are in good consistency with the acoustic simulations, while the grating lobe levels for the lateral deflections are generally higher than those simulated.

To better observe the acoustic field distributions when the focus is deflected laterally, Fig. 7 shows the normalized transversal acoustic pressure distributions with the focus deflected up to ±10 mm in steps of 5 mm on the X-axis, comparing hydrophone measurements and acoustic simulations. As the focal deflection distance increases, both methods show a continuous increase in the levels of the grating lobe and sidelobe. At ±5 mm, hydrophone measurements match well with acoustic simulations, the sidelobe levels are less than 30% and the grating lobe levels are smaller. However, for deflections up to ±10 mm, corresponding to the results in Figs. 6a and 6b, the two-dimensional acoustic field distributions (Figs. 7a and 7e) clearly illustrate that the levels of the grating lobe near the focus are higher and their number is bigger than in the acoustic simulations.

Considering the effectiveness and safety of focused ultrasound, the experimental results indicate that the focal deflection range of this transducer is 40 mm for the Z-axis, 18 mm for the X-axis, and 18 mm for the Y-axis, while lateral deflection is 2 mm smaller than in the acoustic simulations. Therefore, the experimental results of the transducer show good correspondence with the acoustic simulations, especially on the Z-axis. However, the focal deflection is a bit worse on the lateral axis. As shown in Fig. 7, the transversal acoustic pressure distributions at ±10 mm show that the levels of grating lobe near the focus are higher and more numerous compared to the acoustic simulations.

Several possible explanations for this observation can be considered. The presence of the grating lobe is not only related to the focal deflection distance but also to the array structure of the phased array. Theoretically, when the distance between each element center is less than half of the wavelength, there are no grating lobes (Ellens *et al.*, 2015; Hynynen, Jones, 2016). However, this rule leads to a very small element size and an excessive number of elements, and the small size is extremely challenging in terms of transducer fabrication cost and matching. In this study, to improve the focus acoustic pressure, the sector vortex elements are used to maximize the filling factor, and the size of the elements limits the deflection of the focus on the lateral axis. Meanwhile, individual elements must have the same area (Rosnitskiy *et al.*, 2020), and the single area of elements used in this study has a difference of approximately 0.75 mm^2 due to the simulation and fabrication, complicating the matching and having some effect on the acoustic field characteristic or even deteriorating them. Furthermore, among hydrophone measurements, the hydrophone size (Umchid *et al.*, 2009) and the crosstalk between the wires may also have some influence on the acoustic field.

In summary, an advantage of the sector vortex array designed in this work is that the increased filling factor produces higher focal acoustic pressure under the same excitation while maintaining the focal deflection range, especially with no effect on the focal deflection capability on the Z-axis. Even though the acoustic pressure decreases more in the lateral axis, the sector vortex array still maintains higher focal acoustic pressure with the focus deflected up to ±10 mm. Consequently, the design of the sector vortex array is suitable for deep tissue treatment requiring high output power, and the array is found to be able to adequately deflect the focus in three dimensions to cover the required treatment volume. Additionally, the use of only one type of element leads to simpler electrical matching. In this work, the array design is the result of increasing the filling factor while keeping the number of elements fixed, and if a larger focal deflection range and higher output power are required, it is possible to reduce the area of array elements and increase the number of elements.

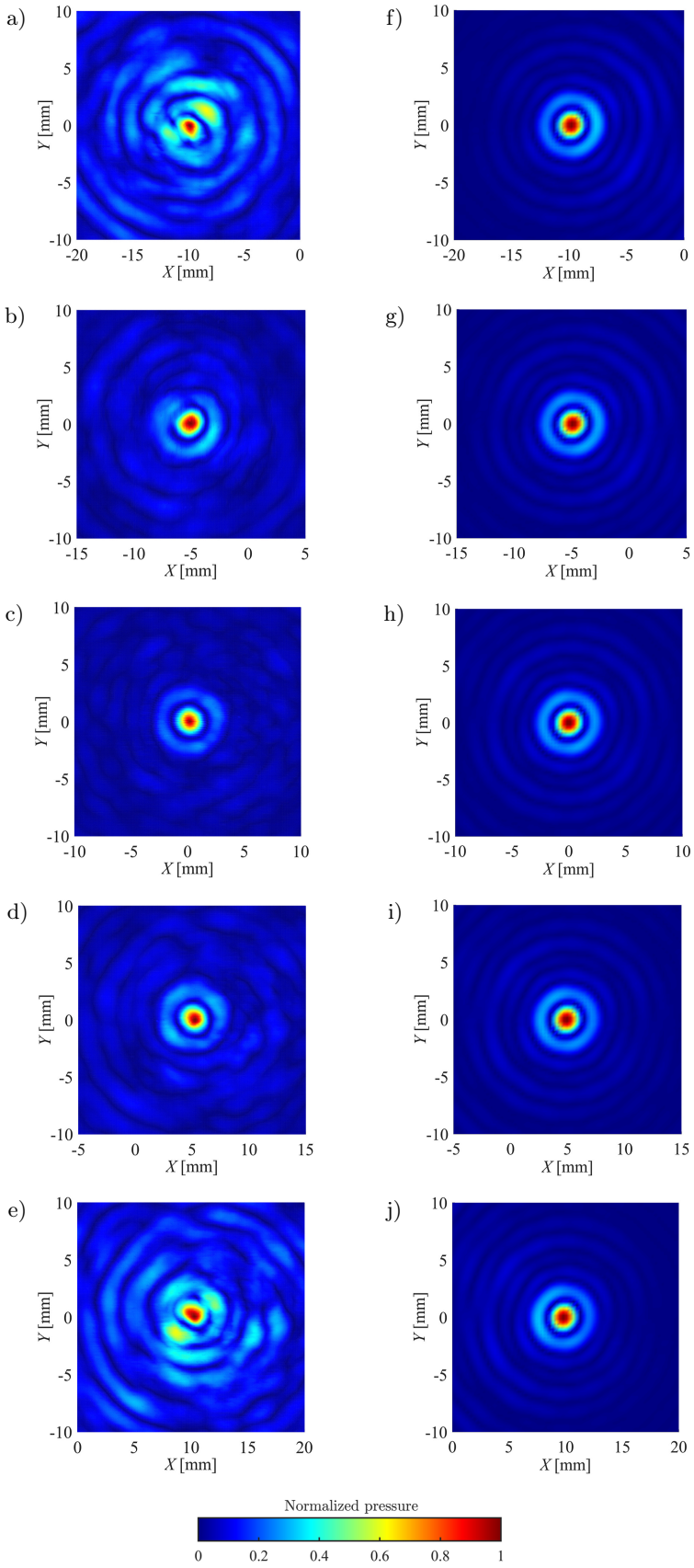

Fig. 7. Illustration of the normalized transversal acoustic pressure distribution with the focus deflected up to ±10 mm in steps of 5 mm and a field of view of 20 × 20 mm, obtained by the hydrophone measurements (a–e), and the acoustic simulations (f–j).

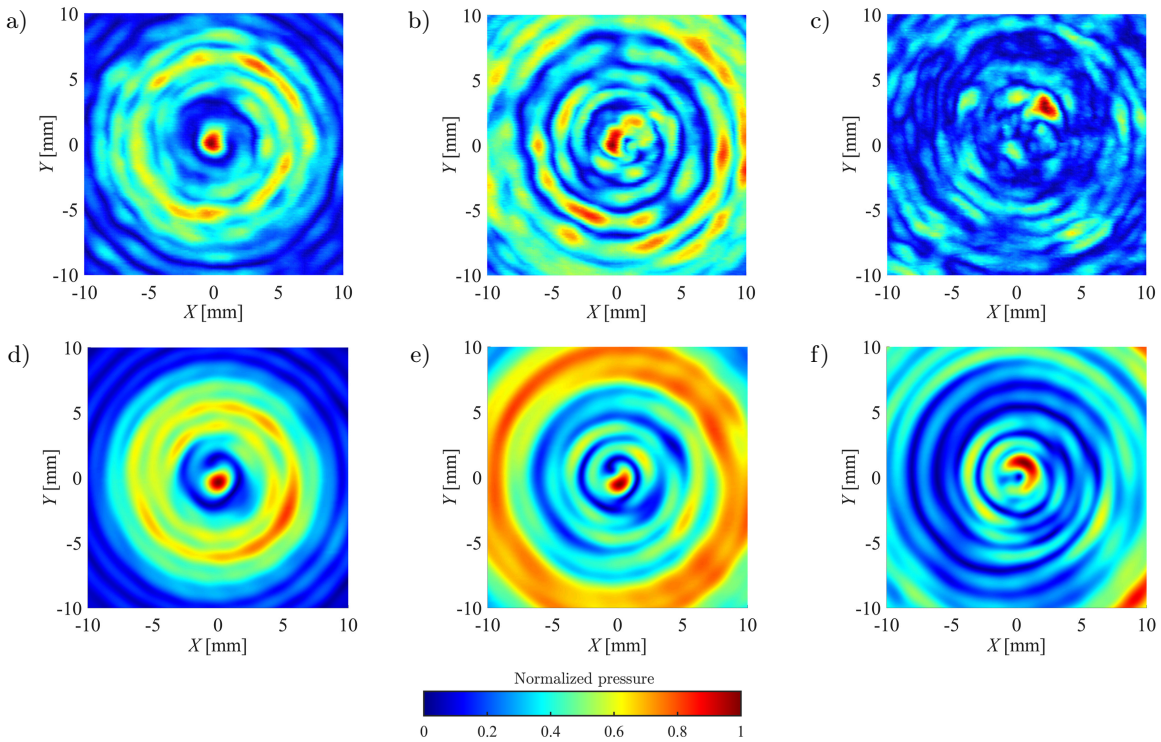

Fig. 8. Illustration of the normalized transversal acoustic pressure distributions in the pre-focal region of 15, 25, and 50 mm, and the field of view of 20 × 20 mm, obtained by the hydrophone measurements (a–c), and the acoustic simulations (d–f).

3.3. Pre-focal acoustic pressure distribution

To observe the pre-focal acoustic field distribution of the transducer, the normalized transversal acoustic pressure distributions were obtained respectively at 15, 25, and 50 mm in the pre-focal region by both hydrophone measurements and acoustic simulations, as shown in Fig. 8. The two methods show good correspondence at the three different distances, and more homogeneous acoustic pressure distributions are observed in the field of view without local hot spots.

In fact, the homogeneous propagation of acoustic pressure generated by the transducer in the pre-focal region, to avoid undesired local hotspots, is also one of the important factors to be considered for the phased array transducer design. Therefore, not only higher focal acoustic pressure and a large focal deflection range are required in evaluating the transducer design, but also avoiding secondary maximum and local hotspots in the pre-focal region (Köhler *et al.*, 2012; Ramaekers *et al.*, 2017a), which is conducive to the safety of clinical treatment. The hydrophone verification of the pre-focal acoustic pressure distributions of the transducer is given in Figs. 8a–c, and the results demonstrate good uniformity and consistency.

4. Conclusion

As a new generation of HIFU transducers – phased arrays offer the advantage of more flexible electronic focusing, higher focal acoustic pressure and a larger focal deflection range, which are critical in clinical applications. This study proposed the design of a sector vortex array based on the Archimedean spiral phased array transducer, which provided the maximum filling factor within the limits of the outer diameter and Archimedean spiral structure while ensuring non-periodic closely filled elements. Considering the safety and effectiveness, the transducer was evaluated through the comparison of hydrophone measurements and acoustic simulations to verify the feasibility of this array design, including the acoustic field distributions of geometric focus, focal deflection capability, and acoustic pressure distributions in the pre-focal region.

The results demonstrated that hydrophone measurements at the geometric focus were in good correspondence with acoustic simulations, and the margin of error was approximately 5%. The transducer's focal deflection capability was nearly identical, with a margin of error of 2%, and the acoustic pressure distributions in the pre-focal region were homogeneous. Therefore, it is indicated that a greater filling factor should be used for designing phased array transducer, enabling higher focal acoustic pressure. The irregular and non-periodic arrangement of the elements can reduce the level of the grating lobe, and the dense filling of elements contributes to the homogeneous distribution of acoustic pressure in the pre-focal region to avoid the local hotspots generated.

In conclusion, the design of the 128-sector vortex Archimedean spiral phased array transducer proposed in this work is suitable for clinical applications requiring high acoustic output power in deep tissues, the lateral focal deflection of ±9 mm and axis focal deflection of ±20 mm are also sufficient for clinical applications.

Declarations

The authors declare that they have no conflicts of interest. This article does not contain any studies with human or animal subjects performed by any of the authors.

References

1. Auboiroux V., Dumont E., Petrusca L., Viallon M., Salomir R. (2011), An MR-compliant phased-array HIFU transducer with augmented steering range, dedicated to abdominal thermotherapy, *Physics in Medicine & Biology*, **56**(12): 3563–3582, doi: 10.1088/0031-9155/56/12/008.
2. Daum D.R., Hynynen K. (1999), A 256-element ultrasonic phased array system for the treatment of large volumes of deep seated tissue, *IEEE Transactions on Ultrasonics, Ferroelectrics, and Frequency Control*, **46**(5): 1254–1268, doi: 10.1109/58.796130.
3. Ebbini E.S., Cain C.A. (1991), A spherical-section ultrasound phased array applicator for deep localized hyperthermia, *IEEE Transactions on Biomedical Engineering*, **38**(7): 634–643, doi: 10.1109/10.83562.
4. Ellens N.P., Lucht B.B., Gunaseelan S.T., Hudson J.M., Hynynen K.H. (2015), A novel, flat, electronically-steered phased array transducer for tissue ablation: Preliminary results, *Physics in Medicine & Biology*, **60**(6): 2195–2215, doi: 10.1088/0031-9155/60/6/2195.
5. Feril L.B., Fernan R.L., Tachibana K. (2021), High-intensity focused ultrasound in the treatment of breast cancer, *Current Medicinal Chemistry*, **28**(25): 5179–5188, doi: 10.2174/0929867327666201111143206.
6. Fukuda H. *et al.* (2011), Treatment of small hepatocellular carcinomas with US-guided high-intensity focused ultrasound, *Ultrasound in Medicine & Biology*, **37**(8): 1222–1229, doi: 10.1016/j.ultrasmedbio.2011.04.020.
7. Gavrilov L.R., Hand J.W. (2000), A theoretical assessment of the relative performance of spherical phased arrays for ultrasound surgery, *IEEE Transactions on Ultrasonics, Ferroelectrics, and Frequency Control*, **47**(1): 125–139, doi: 10.1109/58.818755.
8. Gavrilov L.R., Sapozhnikov O.A., Khokhlova V.A. (2015), Spiral arrangement of elements of two-dimensional ultrasonic therapeutic arrays as a way of increasing the intensity at the focus, *Bulletin of the Russian Academy of Sciences: Physics*, **79**(10): 1232–1237, doi: 10.3103/s106287381510010x.
9. Goss S.A., Frizzell L.A., Kouzmanoff J.T., Barich J.M., Yang J.M. (1996), Sparse random ultrasound phased array for focal surgery, *IEEE Transactions on Ultrasonics, Ferroelectrics, and Frequency Control*, **43**(6): 1111–1121, doi: 10.1109/58.542054.
10. Hynynen K., Jones R.M. (2016), Image-guided ultrasound phased arrays are a disruptive technology for non-invasive therapy, *Physics in Medicine & Biology*, **61**(17): R206, doi: 10.1088/0031-9155/61/17/R206.
11. Köhler M., Mougenot C., Ylihautala M. (2012), Near-field heating of volumetric MR-HIFU hyperthermia, [in:] *11th International Symposium on Therapeutic Ultrasound. AIP Conference Proceedings*, **1481**(1): 180–184, doi: 10.1063/1.4757331.
12. Lean H.Q., Zhou Y. (2019), Acoustic field of phased-array ultrasound transducer with the focus/foci shifting, *Journal of Medical and Biological Engineering*, **39**(6): 919–931, doi: 10.1007/s40846-019-00464-z.
13. Liu Y., Ran W., Shen Y., Feng W., Yi J. (2017), High-intensity focused ultrasound and laparoscopic myomectomy in the treatment of uterine fibroids: A comparative study, *BJOG*, **124**(S3): 36–39, doi: 10.1111/1471-0528.14745.
14. Lu X., Zeng D. (2023), Simulation research on increasing the focus sound pressure of Archimedean spiral phased array transducer [in Chinese], *Technical Acoustic*, **42**(2): 263–268.
15. Morrison K.P., Keilman G.W., Kaczkowski P.J. (2014), Single archimedean spiral close packed phased array HIFU, [in:] *IEEE International Ultrasonics Symposium*, pp. 400–404, doi: 10.1109/ULTSYM.2014.0099.
16. Payne A., Vyas U., Todd N., de Bever J., Christensen D.A., Parker D.L. (2011), The effect of electronically steering a phased array ultrasound transducer on near-field tissue heating, *Medical Physics*, **38**(9): 4971–4981, doi: 10.1118/1.3618729.
17. Raju B.I., Hall C.S., Seip R. (2011), Ultrasound therapy transducers with space-filling non-periodic arrays, [in:] *IEEE Transactions on Ultrasonics, Ferroelectrics, and Frequency Control*, **58**(5): 944–954, doi: 10.1109/tuffc.2011.1895.
18. Ramaekers P., de Greef M., Berriet R., Moonen C.T.W., Ries M. (2017a), Evaluation of a novel therapeutic focused ultrasound transducer based on Fermat's spiral, *Physics in Medicine & Biology*, **62**(12): 5021–5045, doi: 10.1088/1361-6560/aa716c.
19. Ramaekers P., Ries M., Moonen C.T.W., de Greef M. (2017b), Improved intercostal HIFU ablation using a phased array transducer based on Fermat's spiral and Voronoi tessellation: A numerical evaluation, *Medical Physics*, **44**(3): 1071–1088, doi: 10.1002/mp.12082.
20. Rosnitskiy P.B., Sapozhnikov O.A., Gavrilov L.R., Khokhlova V.A. (2020), Designing fully populated

phased arrays for noninvasive ultrasound surgery with controlled degree of irregularity in the arrangement of elements, *Acoustical Physics*, **66**(4): 352–361, doi: 10.1134/s1063771020040090.

21. Rosnitskiy P.B., Vysokanov B.A., Gavrilov L.R., Sapozhnikov O.A., Khokhlova V.A. (2018), Method for designing multielement fully populated random phased arrays for ultrasound surgery applications, *IEEE Transactions on Ultrasonics, Ferroelectrics, and Frequency Control*, **65**(4): 630–637, doi: 10.1109/TUFFC.2018.2800160.

22. Shehata Elhelf I.A., Albahar H., Shah U., Oto A., Cressman E., Almekkawy M. (2018), High intensity focused ultrasound: The fundamentals, clinical applications and research trends, *Diagnostic and Interventional Imaging*, **99**(6): 349–359, doi: 10.1016/j.diii.2018.03.001.

23. Umchid S. *et al.* (2009), Development of calibration techniques for ultrasonic hydrophone probes in the frequency range from 1 to 100 MHz, *Ultrasonics*, **49**(3): 306–311, doi: 10.1016/j.ultras.2008.09.011.

24. Wang J., Sun S., Ning Y., Gong Y., Zhang M., Pang W. (2021), A spiral Archimedean PMUT array with improved focusing performance, [in:] *2021 IEEE International Ultrasonics Symposium (IUS)*, pp. 1–3, doi: 10.1109/IUS52206.2021.9593339.